AFRL-RX-WP-TP-2008-4154

TWO PHASE MONAZITE/XENOTIME 30$LaPO_4$-70YPO_4 COATING OF CERAMIC FIBER TOWS (POSTPRINT)

E.E. Boakye, R.S. Hay, P. Mogilevsky, and M.K. Cinibulk

UES, Inc.

APRIL 2008

AIR FORCE RESEARCH LABORATORY
MATERIALS AND MANUFACTURING DIRECTORATE
WRIGHT-PATTERSON AIR FORCE BASE, OH 45433-7750
AIR FORCE MATERIEL COMMAND
UNITED STATES AIR FORCE

REPORT DOCUMENTATION PAGE

Form Approved
OMB No. 0704-0188

1. REPORT DATE *(DD-MM-YY)*	2. REPORT TYPE	3. DATES COVERED *(From - To)*
April 2008	Journal Article Postprint	

4. TITLE AND SUBTITLE
TWO PHASE MONAZITE/XENOTIME 30$LaPO_4$-70YPO_4 COATING OF CERAMIC FIBER TOWS (POSTPRINT)

5a. CONTRACT NUMBER
FA8650-04-D-5233

5b. GRANT NUMBER

5c. PROGRAM ELEMENT NUMBER
62102F

6. AUTHOR(S)
E.E. Boakye and P. Mogilevsky (UES, Inc.)
R.S. Hay and M.K. Cinibulk (AFRL/RXLN)

5d. PROJECT NUMBER
4347

5e. TASK NUMBER
RG

5f. WORK UNIT NUMBER
M05R1000

7. PERFORMING ORGANIZATION NAME(S) AND ADDRESS(ES)

UES Inc.
Dayton, OH 45432

Ceramics Branch (AFRL/RXLN)
Metals, Ceramics & Nondestructive Evaluation Division
Materials and Manufacturing Directorate
Wright-Patterson Air Force Base, OH 45433-7750
Air Force Materiel Command, United States Air Force

8. PERFORMING ORGANIZATION REPORT NUMBER

9. SPONSORING/MONITORING AGENCY NAME(S) AND ADDRESS(ES)
Air Force Research Laboratory
Materials and Manufacturing Directorate
Wright-Patterson Air Force Base, OH 45433-7750
Air Force Materiel Command
United States Air Force

10. SPONSORING/MONITORING AGENCY ACRONYM(S)
AFRL/RXLN

11. SPONSORING/MONITORING AGENCY REPORT NUMBER(S)
AFRL-RX-WP-TP-2008-4154

12. DISTRIBUTION/AVAILABILITY STATEMENT
Approved for public release; distribution unlimited.

13. SUPPLEMENTARY NOTES
Published in the *Journal of the American Ceramic Society*, Vol. 91, No. 1, pages 17 - 25, 2008. Paper contains color.

14. ABSTRACT
Equiaxed yttrium-lanthanum phosphate nanoparticles ($Y_{0.7}$,$La_{0.3}$)PO_4· 0.7H_2O were made and used to continuously coat Nextel™ 720 fiber tows. The particles were precipitated from a mixture of yttrium and lanthanum citrate chelate and phosphoric acid (H_3PO_4), and characterized with differential thermal analysis and thermogravimetric analysis, X-ray diffraction, transmission electron microscopy, and scanning electron microscopy. The coated fibers were heat treated at 1000–1300 ºC for 1, 10, and 100 h. Coating grain growth kinetics and coated fiber strengths were determined and compared with equiaxed La-monazite coatings. The relationships between coating porosity, coating hermeticity, and coated fiber strength are discussed.

15. SUBJECT TERMS
Ceramic Composites, Fiber Coating

16. SECURITY CLASSIFICATION OF:			17. LIMITATION OF ABSTRACT:	18. NUMBER OF PAGES	19a. NAME OF RESPONSIBLE PERSON (Monitor)
a. REPORT	b. ABSTRACT	c. THIS PAGE			Randall S. Hay
Unclassified	Unclassified	Unclassified	SAR	16	19b. TELEPHONE NUMBER *(Include Area Code)* N/A

Standard Form 298 (Rev. 8-98)
Prescribed by ANSI Std. Z39-18

journal

J. Am. Ceram. Soc., 91 [1] 17–25 (2008)
DOI: 10.1111/j.1551-2916.2007.02005.x

Two Phase Monazite/Xenotime $30LaPO_4$–$70YPO_4$ Coating of Ceramic Fiber Tows

E. E. Boakye,[†,‡] R. S. Hay,[§] P. Mogilevsky,[‡] and M. K. Cinibulk[§]

[‡]UES Inc., Dayton, Ohio 45432

[§]Air Force Research Laboratory, Materials and Manufacturing Directorate (AFRL/MLLN), Wright-Patterson Air Force Base, Ohio 45433

Equiaxed yttrium–lanthanum phosphate nanoparticles ($Y_{0.7}$,$La_{0.3}$)$PO_4 \cdot 0.7H_2O$ were made and used to continuously coat Nextel™ 720 fiber tows. The particles were precipitated from a mixture of yttrium and lanthanum citrate chelate and phosphoric acid (H_3PO_4), and characterized with differential thermal analysis and thermogravimetric analysis, X-ray diffraction, transmission electron microscopy, and scanning electron microscopy. The coated fibers were heat treated at 1000°–1300°C for 1, 10, and 100 h. Coating grain growth kinetics and coated fiber strengths were determined and compared with equiaxed La-monazite coatings. The relationships between coating porosity, coating hermeticity, and coated fiber strength are discussed.

I. Introduction

Monazite ($LaPO_4$) fiber coatings promote crack deflection and fiber pull out in oxide–oxide ceramic-matrix composites (CMCs).[1–5] Two significant fiber coating issues are the thermomechanical stability of fiber coatings controlled by fiber coating coefficient of thermal expansion (CTE) differences,[6,7] and the high-temperature microstructural instability of coatings, principally coating spheroidization enabled by grain growth.[8–11] Large coating-fiber CTE differences promote debonding of coating during fiber handling and CMC processing. Spheroidization of thin coating limits coating coverage and therefore mechanical functionality, and exposes fiber surfaces to environmental effects during processing and use that may degrade fiber strength.[12–15]

The two oxide fibers most suitable for high-temperature structural CMCs are Nextel™ 610, an all alumina fiber with an average CTE of $7.9 \times 10^{-6\circ}C^{-1}$,[16,17] and Nextel™ 720, an alumina-mullite fiber with an average CTE of $6.6 \times 10^{-6\circ}C^{-1}$.[16,17] Both have CTEs lower than monazite ($9.6 \times 10^{-6\circ}C^{-1}$).[1] An oxide coating similar to monazite, but with a lower CTE that is more compatible with Nextel™ 720 is desirable. Xenotime (YPO_4)[18–20] bonds weakly to many oxides and has an average CTE of $6.2 \times 10^{-6\circ}C^{-1}$.[21] There are some reports that compared with monazite, grain growth and sintering of xenotime are slow,[21,22] so the high-temperature microstructural stability of xenotime coatings could be better than that of monazite. Two-phase mixtures of monazite and xenotime can in principle be tailored to match the CTE of Nextel™ 720. An additional possible benefit of two-phase mixtures is further reduction of grain growth rates,[23–25] which in turn promote the high temperature microstructural stability and limit spheroidization of thin fiber coatings.

The formation, characterization, and possible benefits of two-phase monazite/xenotime continuous fiber coatings of ($Y_{0.7}$,$La_{0.3}$)PO_4 bulk composition are reported. Rare-earth phosphates such as monazite, can be synthesized by a variety of wet chemical methods.[26–37] A controlled precipitation method was used to make nano-sized, equiaxed $LaPO_4 \cdot (nH_2O)$ rhabdophane particles by use of lanthanum citrate chelate (La-Cit) and phosphoric acid (H_3PO_4).[7,38,39] The controlled precipitation method was applied to make single phase (Y,La)-$PO_4 \cdot (nH_2O)$ nanoparticles with a high Y content that convert to a two-phase equiaxed monazite/xenotime mixtures after heat treatment above 950°C during fiber coating. The effect of heat treatment temperature on grain growth, coating hermeticity and coated fiber strength is measured and discussed.

II. Experimental Procedure

(1) Materials

Reagent grade lanthanum nitrate hydrate, phosphoric acid, aluminum nitrate nanohydrate (Aldrich Chemical Co., Milwaukee, WI); Yttrium nitrate hexahydrate (Alfa Aesar, Ward Hill MA) and citric acid (CA) (Fisher Scientific Co., Pittsburgh, PA) were used without further purification. The water of hydration of $La(NO_3)_3 \cdot xH_2O$ was determined as 0.6 and that of $Y(NO_3)_3 \cdot 6H_2O$ was confirmed before (Y,La)-rhabdophane synthesis. Water was purified with the nanopure system (Model D4744, Barnstead/Thermolyne Corp., Dubuque, IA) for all experiments.

(2) Precursor Chemistry

Equiaxed hydrated (Y,La)PO_4 nanoparticles were formed by controlled precipitation from yttrium nitrate, lanthanum-nitrate, CA and phosphoric acid as previously done for La-Cit derived rhabdophane.[38] A yttrium–lanthanum citrate mixture (Y,La-Cit) was made by dissolving yttrium nitrate and lanthanum nitrate in ethanol and adding CA to complex the yttrium and lanthanum ions. The yttrium to lanthanum molar ratio was 7:3 and the (Y+La):CA molar ratio was 1:5. Phosphoric acid was added. The P to (Y+La) molar ratios was 1:5. The solution was stirred and equilibrated at ~20°C for 15 min. Rhabdophane precipitation was not observed during the equilibration period. The solution was heated to ~30°C to precipitate (Y,La)$PO_4 \cdot xH_2O$ according to:

$$(Y, La)\text{-Cit} + H_3PO_4 \rightarrow (Y, La)PO_4 \cdot H_2O + H_3Cit \qquad (1)$$

The particles were separated from the supernatant by centrifugation, and washed and redispersed in deionized water to remove residual nitrate and citrate. Washing was repeated until the sol acidity decreased from a pH of <1 to a pH of ~3. Particles dispersed at pH = 3 were not stable; they agglomerated and settled within 3 h. The particles were de-agglomerated by

W. Mullins—contributing editor

Manuscript No. 23142. Received April 27, 2007; approved July 19, 2007.
Work performed under USAF Contract #: F33615-01-C-5214.
[†]Author to whom correspondence should be addressed. e-mail: emmanuel.boakye@wpafb.af.mil

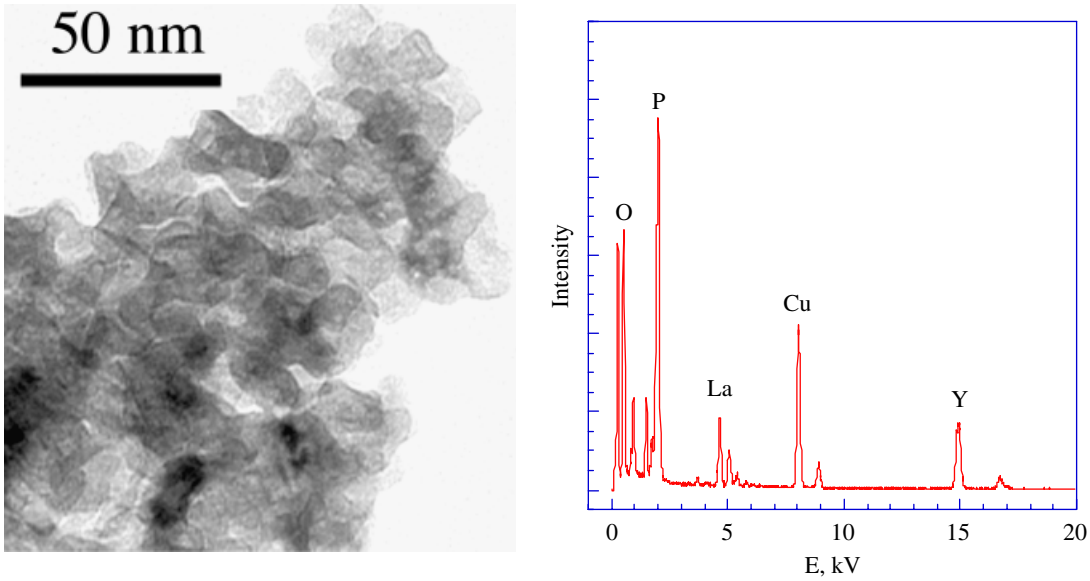

Fig. 1. Transmission electron microscope image and as energy-dispersive X-ray spectrum (EDX) of as precipitated (Y,La)$PO_4 \cdot 0.7H_2O$ particles. EDX simulation showed the Y:La molar ratio to be 70:30.

adding NH_4OH to pH = ~9, and were further dispersed with tetramethyl ammonium hydroxide (TMAH) solution. The pH was determined with a pH/ion meter (Corning Inc., Corning, NY). The dispersed particles were separated by centrifugation, washed and redispersed in deionized water. Washing was repeated until the pH was ~7. The sol was then used for fiber coating. Transmission electron microscope (TEM) images of the coated fibers showed a thin layer of aluminum phosphate ($AlPO_4$) at the fiber coating interface caused by the reaction of the excess phosphorus in the coatings and alumina in the fiber surface (Section III(3) below). To scavenge excess phosphorus, some (Y,La)$PO_4 \cdot H_2O$ sol was doped with 1 wt% Al_2O_3 in the form of aluminum nitrate–citrate. These sols were also used for fiber coating.

(3) Characterization

Differential thermal analysis (DTA) and thermogravimetric analysis (TGA) (Model STA-409, Netzsch-Geratebau Gmbh, Selb, Germany) were done at a heating rate of 10°C/min from 50° to 1400°C in air. Powder samples for DTA and TGA analysis were dried at 140°C for 18 h. X-ray diffraction (XRD) was done with a diffractometer (Rotaflex, Rigaku Co. Tokyo, Japan) after a 1 h heat treatment at 1000°, 1100°, 1200°, 1300°, and 1400°C. Particles were separated with Sorvall Super Centrifuge (Model T21, L.P., Newtown, CT). Particle agglomerate size was measured with a light scattering Particle Size Analyzer (Model N4 Plus Coulter™, Miami, FL). The coatings were examined with a scanning electron microscope (SEM) (Model 360FE Ernst Leitz, Wetzler, Germany) equipped with energy-dispersive X-ray spectrometer (EDX) (ThermoNoran Voyager, Thermo Electron North America LLC, Madison, WI) operating at 15 kV. TEM of the particles and coatings was done with a 200 kV electron microscope (Philips CM200, FEI Co., Hillsboro, OR) equipped with EDS (ThermoNoran Voyager, Thermo Electron North America LLC, Madison, WI). Particles were prepared for TEM analysis by drying sols on TEM grids. Coated fiber cross-section TEM thin foils were made by established methods.[40,41] Single filament tensile strengths and Weibull modulii were measured using a 2.54 cm gauge length. A minimum of 50 tests were done for each data point under the assumption of a uniform fiber diameter.[42]

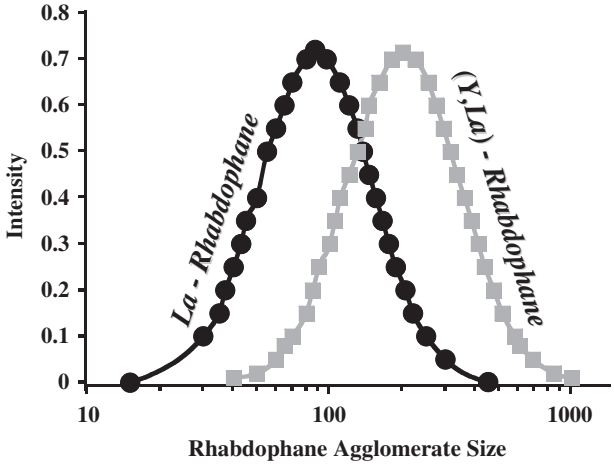

Fig. 2. Particle size distribution for La-rhabdopane and (Y,La) rhabdophane particles measured by light scattering.

(4) Fiber Coating

Nextel™ 720 fiber tows were coated with the hydrated yttrium–lanthanum phosphate [(Y,La)$PO_4 \cdot H_2O$] sol washed to a pH ~7.

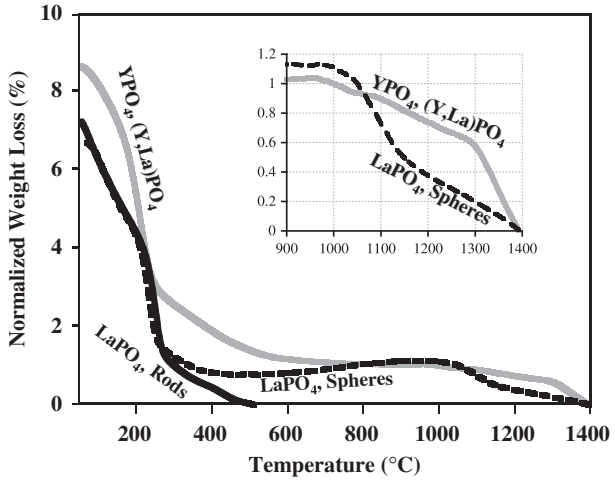

Fig. 3. Thermogravimetric analysis weight loss of rod-shaped La-$PO_4 \cdot XH_2O$, equiaxed $LaPO_4 \cdot XH_2O$ and (Y,La)$PO_4 \cdot XH_2O$. The weight loss is normalized to final monazite weight at 1400°C. Rod-shaped $LaPO_4 \cdot XH_2O$ has a negligible weight loss at the coating temperature of 1100°C. The corresponding weight loss for the equiaxed $LaPO_4 \cdot XH_2O$ and (Y, La) $PO_4 \cdot XH_2O$ are ~0.8% and 0.9%, respectively.

Table I. Thermogravimetric Analysis (TGA) Weight Loss for (Y,La)PO_4 and $LaPO_4$ Precursors

	TGA weight loss% (normalized)		
Temperature (°C)	(Y,La)PO_4	$LaPO_4$-equiaxed	$LaPO_4$-rod-shaped
25–200	5.2	3.8	3.3
1100	0.9	0.7	Negligible

Fibers were desized at 1100°C before coating. A continuous vertical coating apparatus was used in all the coating experiments along with 1-octanol for immiscible liquid displacement.[12] The coating apparatus was similar to that used previously, except that separate vessels housed the coating precursor and the immiscible liquid. Desized tow is wetted by coating precursor as it passes continuously under a teflon pulley. The wetted tows then go under another teflon pulley into 1-octanol, where excess sol within and around the tow is displaced. The wetted tow then moves continuously at 3 cm/s through a vertical tube furnace, where the coatings are heat treated at 1100°C. The furnace hot zone was ~8 cm in length and the total furnace length was 30 cm. The coatings are heated very rapidly and held at maximum temperature for ~3 s. The supply and take up spools are interchanged and the process is repeated up to 6 times to increase coating coverage and thickness.

III. Results

(1) TEM, Light Scattering Particle Size, and EDX Analysis

TEM observation shows (Y,La)-rhabdophane equiaxed particles of 10 nm in diameter (Fig. 1), similar to La-rhabdophane particles.[38] However, light scattering measurements show larger particle sizes of 200 nm (Fig. 2). This suggests that there was significant particle agglomeration in the sols, similar to that inferred for La-rhabdophane.[43] Y to La ratio was analyzed by the standardless EDX method in the TEM using the Voyager software. The analysis yielded an average Y content in the powder of 69.8 at.% (with respect to the total cation content), in good agreement with the 7:3 Y to La molar ratio in which the components were mixed. Also, EDX elemental mapping of the as-precipitated powder revealed no phase separation or compositional inhomogeneity.

(2) TGA/DTA and XRD

The TGA data for (Y,La)PO_4 particles are compared with $LaPO_4$ particles in Fig. 3.[7,38] Data is normalized to the final anhydrous orthophosphate weight at 1400°C. From 50° to 200°C there was a 5.2% weight loss for (Y,La)PO_4, 3.8% weight loss for the equiaxed La-rhabdophane, and 3.3% weight loss for the rod-shaped La-rhabdophane. This is consistent with the known water of hydration of 0.7H_2O for (Y,La)PO_4, 0.6 H_2O for equiaxed $LaPO_4$, and 0.5 H_2O for rod-shaped $LaPO_4$.[13,15,30,31,38,44] Weight loss above 1100°C was negligible for rod-shaped $LaPO_4$, 0.7% for the equiaxed $LaPO_4$ and 0.9% for the (Y,La)PO_4 (Table I). Weight loss for equiaxed La-rhabdophane and (Y,La)PO_4 particles was consistently higher than that for rod-shaped particles above 300°C. This was attributed to the decomposition of absorbed CA and TMAH.[38]

The exothermic DTA peak for dehydration of rhabdophane to monazite was at ~750°C for both equiaxed and rod-shaped $LaPO_4$ precursors.[31,38] The corresponding peak for (Y,La)PO_4 was at ~950°C (Fig. 4). This identification was confirmed by XRD. XRD spectrum of the powder heat-treated at 10°C/min to 860°C was consistent with hexagonal rhabdophane, but with diffraction peaks shifted to higher angles compared with pure La-rhabdophane (Fig. 5). The lattice parameters of the rhabdophane powder were consistent with its composition.[45] Powders heat treated to 950°C had a mixture of monazite and xenotime (Fig. 5). The positions of the monazite diffraction peaks were shifted to higher angles compared with pure La-monazite. From XRD data, the first monazite phase appearing immediately after the 950°C phase transformation from rhabdophane retains most (66 at.% out of ~70 at.% based on the total cation content) of the Y from the parent rhabdophane solid solution.[45] The diffraction patterns of the powder heat treated at 1000°–1600°C also showed monazite peak shifts to higher angles compared with pure $LaPO_4$ monazite.[45] The magnitude of the shift increased with temperature, consistent with increasing solid solubility of Y in monazite at higher temperatures from ~12 at.% at 1000°C to ~42 at.% at 1600°C. The positions of the xenotime diffraction peaks were in good agreement with the PDF data[46] for YPO_4, regardless of the heat treatment. This suggests little solid solubility of La in xeno-

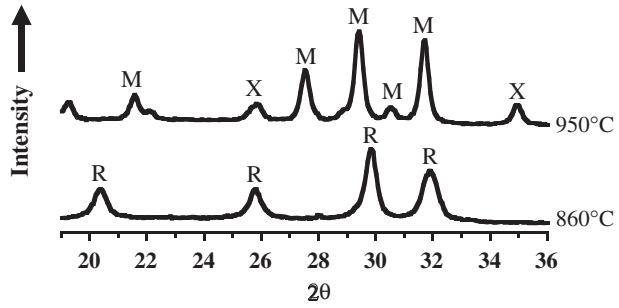

Fig. 5. X-ray diffraction of (Y,La)PO_4 precursor heat treated to 860°C and 950°C.

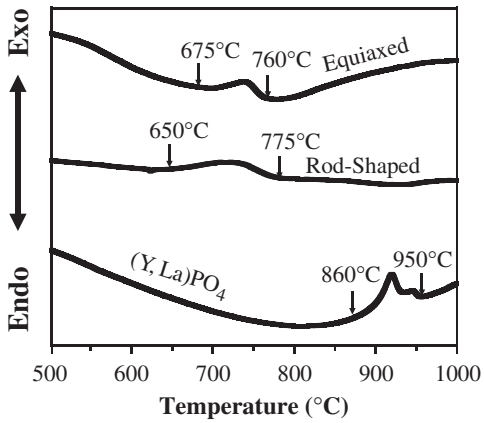

Fig. 4. Differential thermal analysis showing exothermic peak temperatures for $LaPO_4 \cdot XH_2O$ and (Y,La)$PO_4 \cdot XH_2O$ at ~750°C and 950°C, respectively.

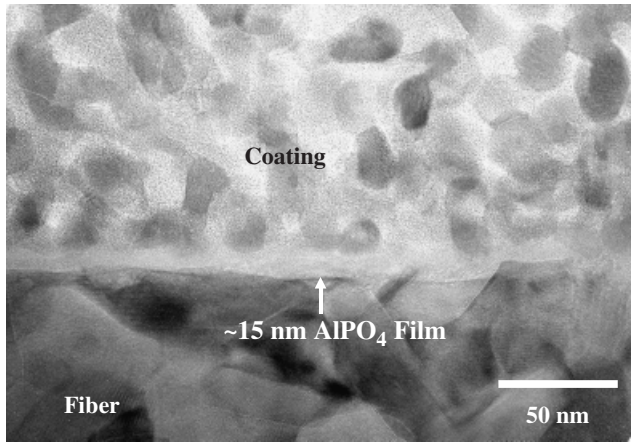

Fig. 6. Transmission electron micrograph of as-deposited (Y,La)PO_4 fiber coatings on Nextel 720, showing a thin film of $AlPO_4$ in the coating fiber interphase.

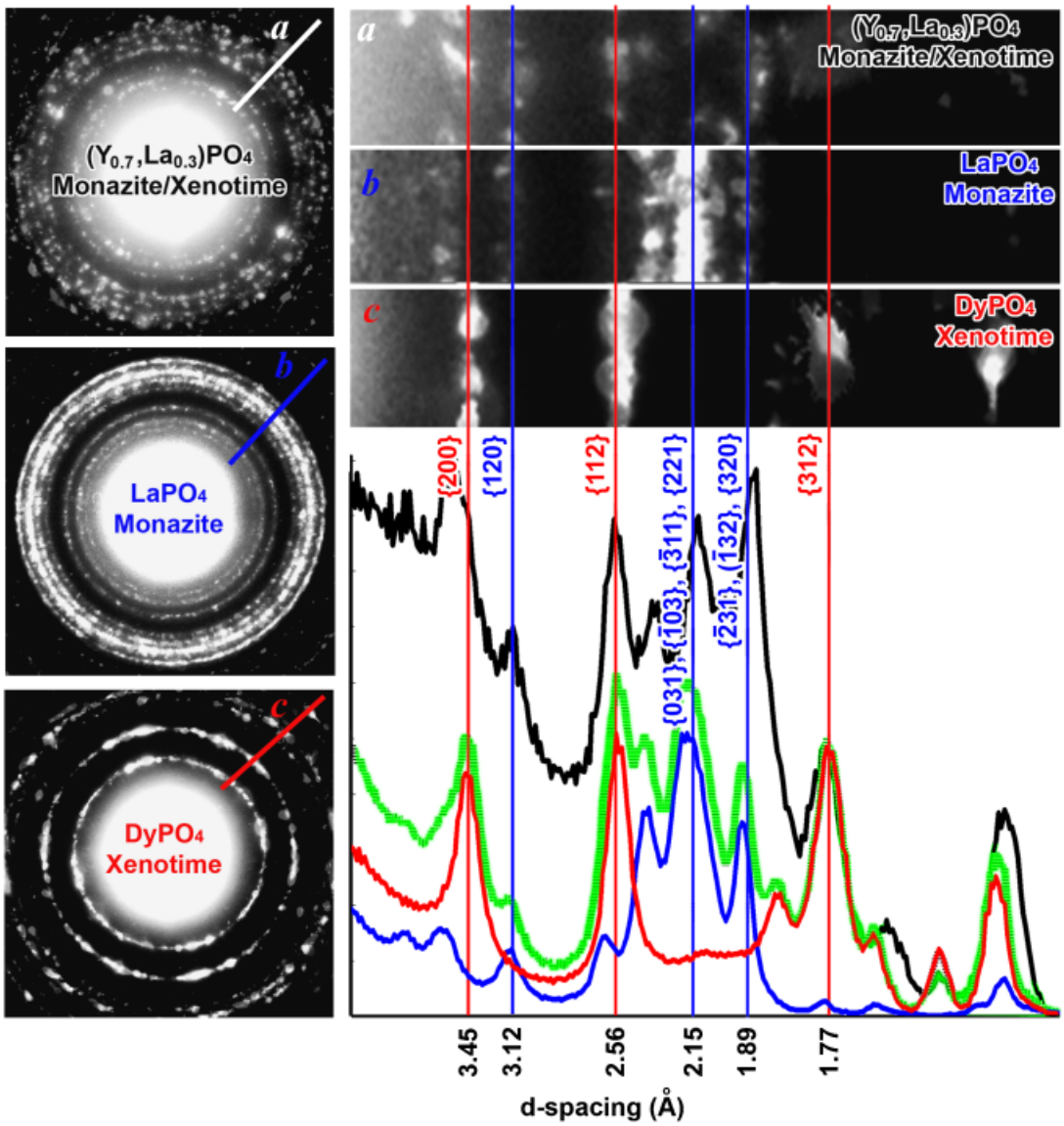

Fig. 7. Transmission electron micrograph and electron diffraction patterns of fiber coatings of $(Y_{0.7}La_{0.3})PO_4$, $DyPO_4$ (xenotime) and $LaPO_4$ (monazite) heat treated at 1200°C/10 h. Prominent rings are identified as monazite (blue) and xenotime (red).

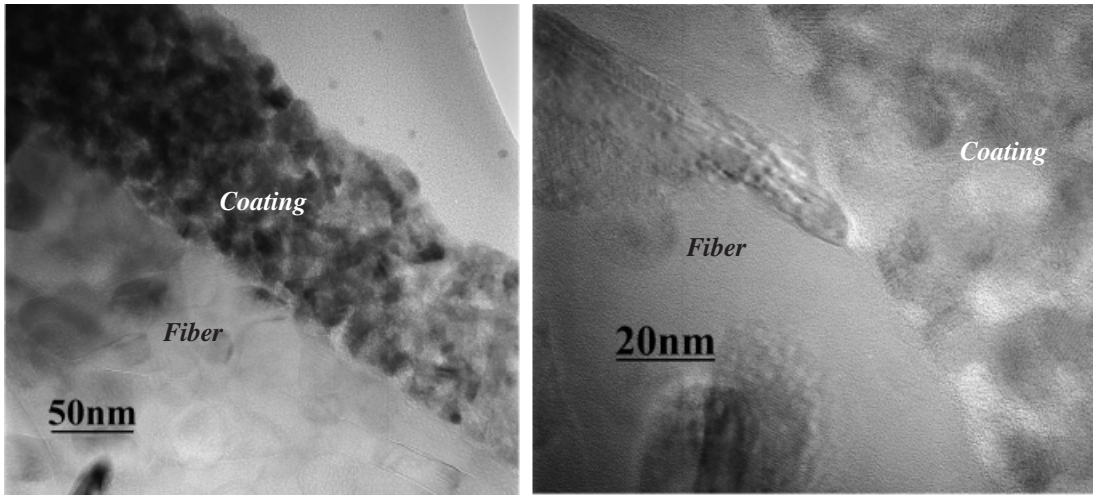

Fig. 8. Transmission electron micrograph of $[(Y,La)PO_4+1\%\ Al_2O_3]$ coating on Nextel 720 showing a clean fiber coating interface.

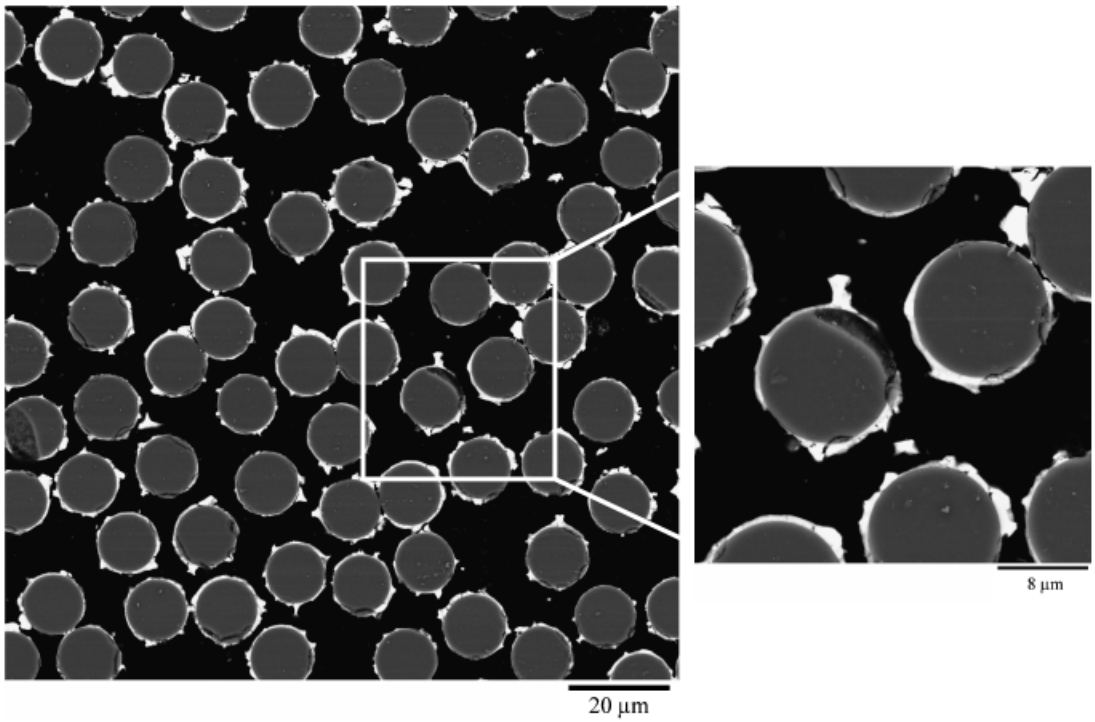

Fig. 9. Cross-sectional scanning electron micrographs of [(Y,La)PO_4+1% Al_2O_3] coating on Nextel 720 fibers.

time.[45] The detailed analysis of the effect of heat-treatment temperatures and time on lattice parameters, phases, and compositions is presented elsewhere.[45]

(3) Fiber Coating

Similar to the spherical La-monazite coatings,[47] grains in the (Y,La)-monazite/xenotime coating were equiaxed and averaged 13 ± 0.7 nm in diameter (Fig. 6). This grain size was slightly larger than the particle size (10 ± 0.5 nm) in the (Y,La)$PO_4 \cdot H_2O$ sol, suggesting minor growth during fiber coating. A semi-quantitative evaluation of the Y to La molar ratio in the coatings was done. Selected area electron diffraction pattern of the fiber coating heat treated at 1200°C for 10 h (Fig. 7(a), left side) was compared with the diffraction patterns from pure monazite and pure xenotime coatings as standards (Fig. 7(b) and (c), respectively). Because pure YPO_4 xenotime coatings were not available, a diffraction pattern from a $DyPO_4$ xenotime coating obtained using the method[48] was used in this analysis. Each pattern in Fig. 7 is a digital summation of eight individual patterns from coatings on different filaments. An enlargement of a strip of each pattern is shown in the upper right hand corner, and the integrated diffraction intensity of the entire pattern is shown in the lower right hand corner over the same *d*-spacing range (monazite—blue, xenotime—red). A digital summation 50–50 (weighting) of the monazite and xenotime patterns

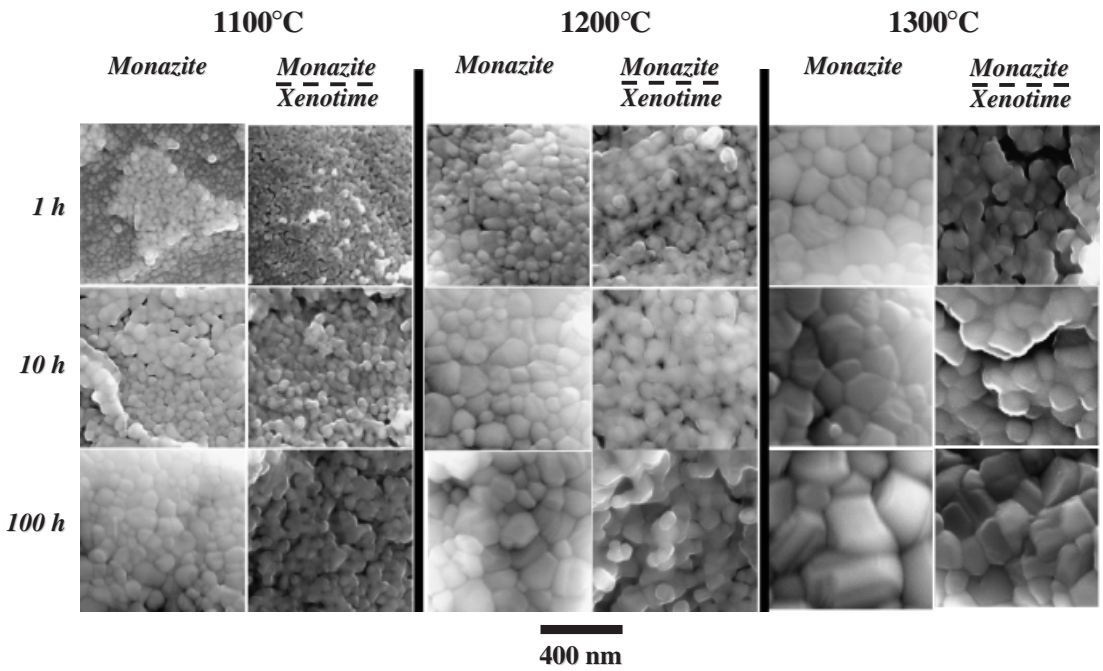

Fig. 10. Scanning electron micrographs of thick equiaxed $LaPO_4$ and (Y,La)PO_4 fiber coatings heat treated from 1 to 100 h at 1100°–1300°C, showing higher grain growth rates of monazite.

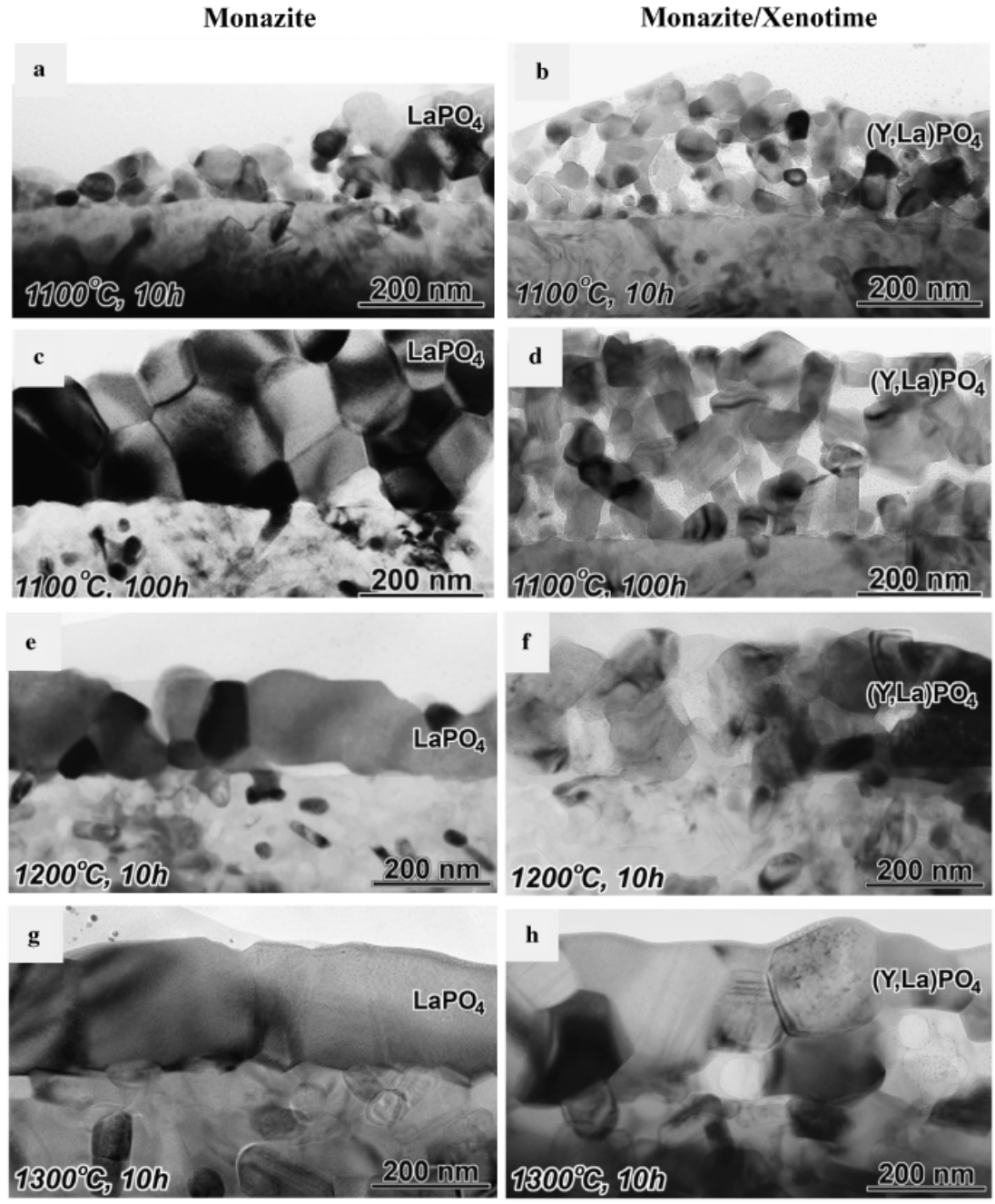

Fig. 11. Transmission electron micrographs of equiaxed $LaPO_4$ and $(Y,La)PO_4$ in cross section after heat treatment at 1100°, 1200°, and 1300°C for 10–100 h. Monazite coatings are locally hermetic for heat-treatment temperatures >1100°C and time >10 h. Monazite/xenotime coatings heat treated at temperatures up to 1100°C and time 100 h are not hermetic.

(the green line) is shown for comparison with the actual (Y,La)-monazite/xenotime pattern (the black line). Prominent monazite and xenotime rings are identified with the *d*-spacings. As expected, some of the *d*-spacings were slightly shifted in the (Y,La)-monazite solid-solution. Both monazite and xenotime are present in the (Y,La) monazite/xenotime coating in roughly equal amounts.

A thin film of amorphous $AlPO_4$ was present at the fiber/coating interface (Fig. 6). Trace amorphous $AlPO_4$ was previously observed in fiber coatings made from rod-shaped rhabdophane particles, and was inferred to form by reaction of slight excess coating phosphorous with Al_2O_3 in the fibers.[13] In coatings made with 1 wt% alumina doped sols, $AlPO_4$ films were not observed at the fiber-coating interface (Fig. 8). SEM observations show significant variations in coating thickness $\sim$2 μm to $\sim$50 nm along and between fiber filaments (Fig. 9).

(4) Coating Grain Growth $LaPO_4$ and $(Y, La)PO_4/YPO_4$

Grain growth of (Y,La)-monazite/xenotime coatings heat treated at 1100°–1300°C for 1, 10, and 100 h is compared with $LaPO_4$ coatings made from similar precursors[39] (Figs. 10–13). TEM and SEM observations show slower grain growth rates in (Y,La)-monazite/xenotime coatings (Figs. 10 and 11). The grain growth kinetics was evaluated using SEM data from Table II, the results of which are shown in Fig. 12. The growth kinetics was represented by an equation of the form[49]:

$$d - d_o = k(T)t^n \quad (2)$$

Table II. Average Grain Size (nm) in Monazite (M) and Monazite/Xenotime (M/X) Coatings

	T							
	1000°C		1100°C		1200°C		1300°C	
t	M	M/X	M	M/X	M	M/X	M	M/X
1 h	35	37	53	47	140	96	268	157
10 h	45	41	76	63	200	130	314	213
100 h	48	45	93	75	256	156	597	302

where d_o is the initial and d is the final grain size, $k(T)$ is a temperature dependent growth constant, t is time, and n is a growth exponent (Fig. 12). The growth exponents for monazite (0.10–0.23) were consistently larger than those for monazite–xenotime mixtures (0.08–0.12). All measured growth exponents were much smaller than those observed for Ce-monazite (0.5)[50] and Er-xenotime (0.33).[51] YPO_4 xenotime sintering rates are reported to be lower than those for $LaPO_4$ monazite.[22] Coating porosity and thin film constraints may be at least partly responsible for the low growth exponents.[52,53] Also, two-phase mixtures may alter the grain growth rates by grain boundary pinning or Zener pinning.[53–57] But in this particular situation the Zener model was not applied due to the following reasons: Experimental evidence shows that during heat treatment, the YPO_4 phase forms a solid solution with the $LaPO_4$ phase. Powders heat treated at 1000°C for 100 h had 16.2 at.wt% of Y dissolved in $LaPO_4$. Also, powders heat treated at 1400°C for 1 h had 33.3 at.wt% of Y in $LaPO_4$.[45] The volume fraction of $LaPO_4$ will therefore vary with the heat treatment time and temperature. In addition, the grain growth study show that both the YPO_4 and $LaPO_4$ phase grow whereas in the Zener model the inclusion is assumed to be inert and its size is fixed. Finally the kinetics of growth of xenotime are slower than that of monazite.[21,22,50,51]

$k(T)$ is expressed by the usual Arrhenius equation:

$$k(T) = ce^{-Q/RT} \tag{3}$$

where Q is an activation energy, R is the gas constant, T is the temperature (°K) and c is a rate constant. Arrhenius plots of $[\ln(d-d_o)-n\ln(t)]$ vs. $1/T$ for monazite and (Y,La)-monazite/xenotime grain growth are shown in Fig. 13. Q for monazite grain growth was 135 and 109 kJ/mol for monazite/xenotime grain growth. These values were smaller than those found for $CePO_4$ monazite (192 kJ/mol) and $ErPO_4$ xenotime (159 kJ/mol).

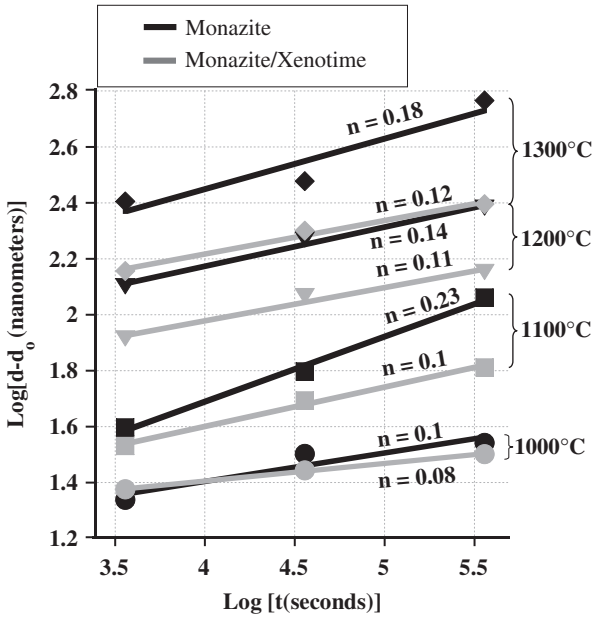

Fig. 12. Isothermal grain growth in thick equiaxed $LaPO_4$ and (Y,La)PO_4 fiber coatings heat treated at 1000°–1300°C for 1–100 h. Growth exponents are shown on the graph for each heat-treatment temperature.

(5) Coated Fiber Strength

The cause of fiber strength degradation during fiber coating has been inferred to be high temperature stress corrosion from coating precursor decomposition products trapped in the coating (Table I and Fig. 3).[7,12–15,39,58,59] For rod-shaped La-rhabdophane, high as-coated fiber strength correlated with low precursor weight loss at high temperatures. As-coated fibers made with equiaxed La-rhabdophane precursor had high as-coated strength despite significant precursor weight loss above 1100°C[39] (Table I, Figs. 3 and 14). However, unlike rod-shaped precursor, the fibers coated with equiaxed monazite had a considerable strength loss after long-term heat treatment for 100 h at 1100°C. Similar to equiaxed La-rhabdophane coated fibers, monazite/xenotime as-coated fibers made with the equiaxed (Y,La)-rhabdophane precursors had high as-coated strength despite significant precursor weight loss above 1100°C (Table I, Figs. 3 and 14). However, their response to long-term heat treatment was rather similar to the rod-shaped pure La-monazite coatings. These fibers retained their high strength after heat treatment for 100 h at 1100°C (Fig. 14).[13,14,39] Nextel™ 720 fibers previously coated with rod-shaped $LaPO_4$ had strengths of $\sim 1.75 \pm 0.05$ GPa after 1100°C/100 h heat-treatment (Fig. 14). The corresponding values for equiaxed monazite and (Y,La)-monazite/xenotime mixtures were 1.38 ± 0.06 GPa and 1.76 ± 0.05 GPa. The corresponding strength of uncoated fiber was 1.80 ± 0.07 GPa.

SEM and TEM studies of the coated fibers heat treated at 1100°C/100 h showed the equiaxed monazite coatings to densify

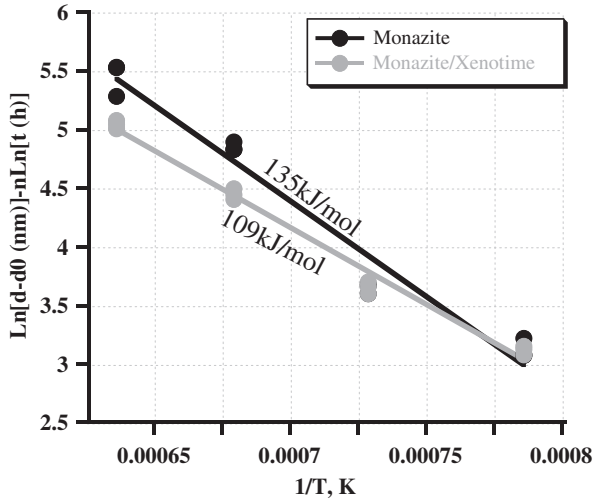

Fig. 13. Arrhenius plots of equiaxed $LaPO_4$ and (Y,La)PO_4 grain growth for 1, 10, 100 h showing the calculated activation energies.

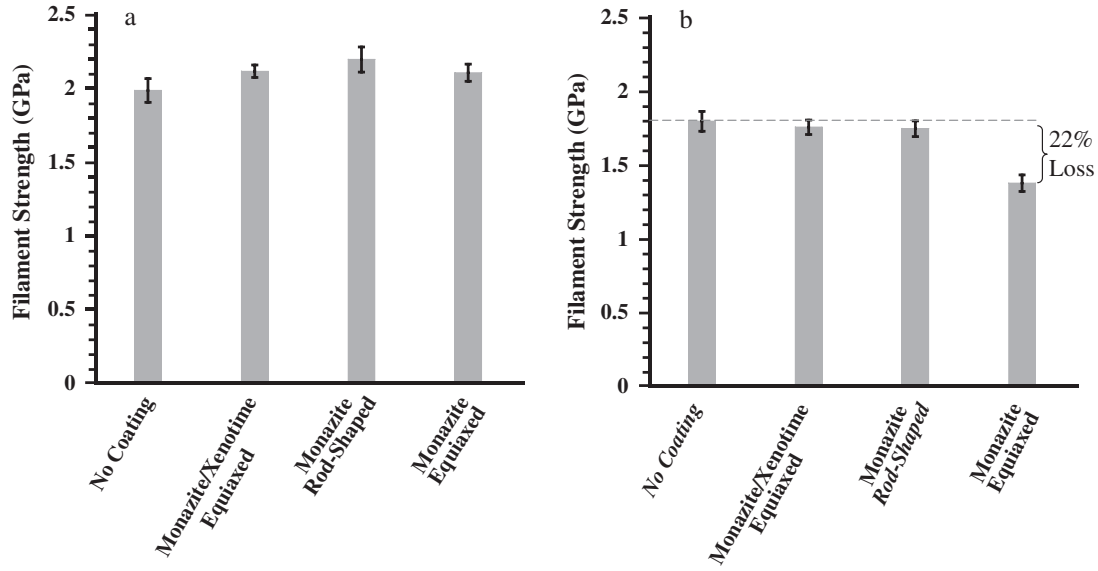

Fig. 14. Tensile strengths of equiaxed $LaPO_4$ coated Nextel 720 fibers; (a) as-coated fiber and (b) heat treated at 1100°C/100 h.

after heat treatment at 1100°C/100 h, whereas the monazite/xenotime coating given a similar heat treatment does not (Fig. 11). In principle dramatic grain growth rate changes are expected as the rate controlling mechanism changes from coarsening by surface diffusion in porous non-hermetic coatings to grain boundary and lattice diffusion in denser coatings. This transition is diagnostic of open porosity transitioning to closed porosity in the coatings. This transition was not observed for either monazite or monazite/xenotime grain growth exponents or activation energies from 1000° to 1300°C (Figs. 12 and 13), although TEM observations of coatings heat treated at 1100°C/100 h showed the monazite coatings to be at least locally hermetic and monazite/xenotime coatings to be non hermitic (Fig. 11).

A tentative explanation for the strength loss after long-term heat treatment for coated fiber made from equiaxed La-rhabdophane may relate to the high surface area and high sintering rate of equiaxed particles (Figs. 10–12). Equiaxed particles may adsorb more precursor decomposition products than rods of the same diameter. These desorb at higher temperatures. Some decomposition products may be trapped in coating pores adjacent to the fiber, and cause growth of fiber surface flaws by stress corrosion cracking driven by intergranular residual stress. The two-phase monazite/xenotime coatings was non hermetic (Fig. 11). Hence the less rapid densification of the two-phase coatings may trap a smaller amount of decomposition products adjacent to the fiber. Therefore, strength degradation by the two-phase coating was less severe.

IV. Conclusions

A single precursor two-phase monazite-xenotime mixture $(Y,La)PO_4 \cdot 0.7H_2O$ was made and used to coat Nextel 720 fiber tows. The precursor was characterized by TGA/DTA and XRD studies before fiber coatings. The precursor transformed to a mixture of a (Y, La)-monazite and xenotime at ~950°C. Coatings heat treated in-line at 1100°C formed a mixture of monazite/xenotime with a ~13 nm grain size.

Grain growth of two-phase monazite/xenotime coatings was slower than that of pure monazite coatings. The growth exponents for monazite ($LaPO_4$) were consistently larger than those for monazite–xenotime [$(Y,La)PO_4/YPO_4$] mixtures. As-coated fiber strength was not degraded by the monazite/xenotime coating derived from nanosized equiaxed particles, despite significant weight loss from the coating precursor at high temperature. After heat treatment at 1100°C/100 h, the monazite/xenotime-coated fiber retained strength, while the monazite coated fiber was degraded in strength. Coated fiber strength loss may be related to the relative densification rates of the two coatings.

References

[1]P. E. D. Morgan and D. B. Marshall, "Ceramic Composites of Monazite and Alumina," *J. Am. Ceram. Soc.*, **78**, 1553–63 (1995).
[2]K. A. Keller *et al.*, "Effectiveness of Monazite Coatings in Oxide/Oxide Composites After Long Term Exposure at High Temperature," *J. Am. Ceram. Soc.*, **86**, 325–32 (2003).
[3]P.-Y. Lee, M. Imai, and T. Yano, "Effects of Sintering Condition on Mechanical Properties of Monazite-Coated Alumina-Fiber/Alumina-Matrix Composites Fabricated by Hot-Pressing," *J. Ceram. Soc. Japan*, **112**, 29–34 (2004).
[4]R. J. Kerans, R. S. Hay, T. A. Parthasarathy, and M. K. Cinibulk, "Interface Design for Oxidation Resistant Ceramic Composites," *J. Am. Ceram. Soc.*, **85**, 2599–632 (2002).
[5]F. W. Zok, "Developments in Oxide Fiber Composites," *J. Am. Ceram. Soc.*, **89**, 3309–24 (2006).
[6]A. G. Evans and J. W. Hutchinson, "Overview No. 120, The Thermomechanical Integrity of Thin Films and Multilayers," *Acta Metall. Mater.*, **43**, 2507–30 (1995).
[7]E. E. Boakye, P. Mogilevsky, J. Welter, R. S. Hay, and R. J. Kerans, "Monazite Coatings on SiC Fibers I: Fiber Strength and Thermal Stability," *J. Am. Ceram. Soc.* **89** [11], 3475–80 (2006).
[8]D. J. Srolovitz and S. A. Safran, "Capillary Instabilities in Thin Films. I. Energetics," *J. Appl. Phys.*, **60**, 247–54 (1986).
[9]D. J. Srolovitz and S. A. Safran, "Capillary Instabilities in Thin Films. II. Kinetics," *J. Appl. Phys.*, **60**, 255–60 (1986).
[10]K. T. Miller, F. F. Lange, and D. B. Marshall, "The Instability of Polycrystalline Thin Films: Experiment and Theory," *J. Mater. Res.*, **5**, 151–60 (1990).
[11]E. Werner, "The Spheroidization of Thin Plates," *Acta. Metall.*, **37**, 2047–53 (1989).
[12]E. Boakye, R. S. Hay, and M. D. Petry, "Continuous Coating of Oxide Fiber Tows Using Liquid Precursors: Monazite Coatings on Nextel 720," *J. Am. Ceram. Soc.*, **82**, 2321–31 (1999).
[13]E. E. Boakye, R. S. Hay, P. Mogilevsky, and L. M. Douglas, "Monazite Coatings on Fibers: II, Coating without Strength Degradation," *J. Am. Ceram. Soc.*, **84**, 2793–801 (2001).
[14]E. E. Boakye and P. Mogilevsky, "Fiber Strength Retention of La and Ce-PO_4 Coated Nextel™ 720," *J. Am. Ceram. Soc.*, **87**, 314–6 (2004).
[15]R. S. Hay and E. Boakye, "Monazite Coatings on Fibers: I, Effect of Temperature and Alumina Doping on Coated Fiber Tensile Strength," *J. Am. Ceram. Soc.*, **84**, 2783–92 (2001).
[16]D. M. Wilson, "New High Temperature Oxide Fibers," pp. 1–12 in *High Temperature Ceramic Matrix Composites*, Edited by W. Krenkel and R.H.N. Schneider. Wiley-VCH, Weinheim, Germany, 2001.
[17]D. M. Wilson and L. R. Visser, "High Performance Oxide Fibers for Metal and Ceramic Composites," *Composites A*, **A32**, 1143–53 (2001).
[18]D.-H. Kuo and W. M. Kriven, "Characterization of Yttrium Phosphate and a Yttrium Phosphate/Yttrium Aluminate Laminate," *J. Am. Ceram. Soc.*, **78**, 3121–4 (1995).
[19]D. B. Marshall, J. B. Davis, P. E. D. Morgan, and J. R. Porter, pp. 27–36, *Key Engineering Materials*. Trans Tech Publications, Switzerland, 1997.

[20]P. E. D. Morgan and D. B. Marshall, "Functional Interfaces for Oxide/Oxide Composites," *Mater. Sci. Eng.*, **A162**, 15–25 (1993).
[21]Y. Hikichi, T. Ota, K. Daimon, T. Hattori, and M. Mizuno, "Thermal, Mechanical, and Chemical Properties of Sintered Xenotime-Type RPO_4 (R = Y, Er, Yb, or Lu)," *J. Am. Ceram. Soc.*, **81**, 2216–8 (1998).
[22]D. Bregiroux, S. Lucas, E. Champion, F. Audubert, and D. Bernache-Assollant, "Sintering and Microstructure of Rare Earth Phosphate Ceramics $REPO_4$ with *RE* = La, Ce, or Y," *J. Eur. Ceram. Soc.*, **26**, 279–87 (2006).
[23]K. B. Alexander, P. F. Becher, S. B. Waters, and A. Bleier, "Grain Growth Kinetics in Alumina-Zirconia (CeZTA) Composites," *J. Am. Ceram. Soc.*, **77**, 939–46 (1994).
[24]J. D. French, M. P. Harmer, H. M. Chan, and G. A. Miller, "Coarsening Resistant Dual Phase Interpenetrating Microstructures," *J. Am. Ceram. Soc.*, **73**, 2508–10 (1990).
[25]F. F. Lange and M. M. Hirlinger, "Grain Growth in Two-Phase Ceramics: Al_2O_3 Inclusions in ZrO_2," *J. Am. Ceram. Soc.*, **70**, 827–30 (1987).
[26]L. Bo, S. Liya, L. Xiaozhen, Z. Shuihe, W. Chunfang, and L. Wenjing, "Monazite Coatings on Short Alumina Fibers Using Layer-by-Layer Assemby Technique," *Mater. Sci. Eng.*, **A354**, 324–32 (2004).
[27]V. Buissette, M. Moreau, T. Gacoin, and J.-P. Boilot, "Luminescent Core/Shell Nanoparticles with a Rhabdophane $LnPO_4.xH_2O$ Structure: Stabilization of Ce^{3+}-Doped Compositions," *Adv. Funct. Mater.*, **16**, 351–5 (2006).
[28]V. Buissette, M. Moreau, T. Gacoin, and J.-P. Boilot, "Colloidal Synthesis of Luminescent Rhabdophane $LaPO_4:Ln^{3+}.xH_2O$ (Ln = Ce, Tb, Eu; $x = 0.7$) Nanocrystals," *Chem. Mater.*, **16**, 3767–73 (2004).
[29]H.-K. Jung, J.-S. Oh, S. Seok, and T.-H. Lee, "Preparation and Luminescence Properties of LaPO4:Er,Yb Nanoparticles," *J. Lumin.*, **114**, 2005 (2005).
[30]S. Lucas, E. Champion, D. Bernache-Assolant, and G. Leroy, "Rare Earth Phosphate Powders $RePO_4.nH_2O$ (Re = La, Ce, or Y) – Part II. Thermal Behavior," *J. Solid-State Chem.*, **177**, 1312–20 (2004).
[31]S. Lucas, E. Champion, D. Bregiroux, D. Bernache-Assolant, and F. Audubert, "Rare Earth Phosphate Powders $RePO_4.nH_2O$ (Re = La, Ce, or Y) – Part I. Synthesis and Characterization," *J. Solid-State Chem.*, **177**, 1302–11 (2004).
[32]T. Masui, H. Tategaki, S. Furukawa, and N. Imanaka, "Synthesis and Characterization of New Environmentally-Friendly Pigments Based on Cerium Phosphate," *J. Ceram. Soc. Japan*, **112**, 646–9 (2004).
[33]J. M. Nedelec, D. Avignant, and R. Mahiou, "Soft Chemistry Routes to YPO4-Based Phosphors: Dependence of Textural and Optical Properties on Synthesis Pathways," *Chem. Mater.*, **14**, 651–5 (2002).
[34]J. M. Nedelec, C. Mansuy, and R. Mahiou, "Sol–Gel Derived YPO4 and LuPO4 Phosphors, a Spectroscopic Study," *J. Mol. Str.*, **651–653**, 165–70 (2003).
[35]H. Onoda, H. Nariai, H. Maki, and I. Motooka, "Syntheses of Various Rare Earth Phosphates from Some Rare Earth Compounds," *Mater. Chem. Phys.*, **73**, 19–23 (2002).
[36]K. Rajesh, P. Mukundan, P. K. Pillai, V. R. Nair, and K. G. K. Warrier, "High-Surface-Area Nanocrystalline Cerium Phosphate through Aqueous Sol–Gel Route," *Chem. Mater.*, **16**, 2700–5 (2004).
[37]K. Rajesh *et al.*, "Synthesis of Nanocrystalline Lanthanum Phosphate for Low Temperature Densification to Monazite Ceramics," *Mater. Lett.*, **58**, 1687–91 (2004).
[38]E. E. Boakye, P. Mogilevsky, and R. S. Hay, "Synthesis of Spherical Rhabdophane Particles," *J. Am. Ceram. Soc.*, **88**, 2740–6 (2005).
[39]E. E. Boakye, R. S. Hay, and P. Mogilevsky, "Spherical Rhabdophane Sols II. Fiber Coating," *J. Am. Ceram. Soc.*, **90** [5], 1580–8 (2007).
[40]R. S. Hay, J. R. Welch, and M. K. Cinibulk, "TEM Specimen Preparation and Characterization of Ceramic Coatings on Fiber Tows," *Thin Solid Films*, **308-309**, 389–92 (1997).
[41]M. K. Cinibulk, J. R. Welch, and R. S. Hay, "Method for Preparation of TEM Specimens of Coated Fibers," *J. Am. Ceram. Soc.*, **79**, 2481–4 (1996).
[42]M. D. Petry, T. Mah, and R. J. Kerans, "Validity of Using Average Diameter for Determination of Tensile Strength and Weibull Modulus of Ceramic Filaments," *J. Am. Ceram. Soc.*, **80**, 2741–4 (1997).
[43]E. E. Boakye, R. S. Hay, and P. Mogilevsky, "Spherical Rhabdophane Sols II. Fiber Coating," *J. Am. Ceram. Soc.*, **90**, 1580–8 (2007).
[44]W. Min, K. Daimon, T. Ota, T. Matsubara, and Y. Hikichi, "Synthesis and Thermal Reactions of Rhabdophane-(Yb or Lu)," *Mater. Res. Bull.*, **35**, 2199–205 (2000).
[45]P. Mogilevsky, E. E. Boakye, and R. S. Hay, "Solid Solubility and Thermal Expansion in $LaPO_4$–YPO_4 System," *J. Am. Ceram. Soc.*, **90**, 1899–907 (2006).
[46]M. K. Carron, C. R. Naeser, H. J. Jr. Rose, and F. A. Hildebrand, "Fractional Precipitation of Rare Earth with Phosphoric Acid," *U. S. Geol. Surv. Bull.*, 1036, 253–275 (1958).
[47]E. E. Boakye, R. S. Hay, and P. Mogilevsky, "Spherical Rhabdophane Sols II. Fiber Coating," *J. Am. Ceram. Soc.*, **90** [5], 1580–8 (2007).
[48]G. F. Fair, R. S. Hay, and E. E. Boakye, "Precipitation Coating of Monazite on Woven Ceramic Fibers: I. Feasibility," *J. Am. Ceram. Soc.*, **90**, 448–55 (2006).
[49]J. W. Martin, R. D. Doherty, and B. Cantor, "Microstructural change due to Grain Boundary Energies", pp. 307–66 in *Stability of Microstructure in Metallic Systems*, Edited by R. W. Cahn. University Press, Cambridge, 1997.
[50]Y. Hikichi, T. Nomura, Y. Tanimura, S. Suzuki, and M. Miyamoto, "Sintering and Properties of Monazite-Type $CePO_4$," *J. Am. Ceram. Soc.*, **73**, 3594–6 (1990).
[51]I. A. Bondar, A. I. Domanski, L. P. Mezentseva, M. G. Degen, and N. E. Kalinina, "A Physicochemical Study of Lanthanide Orthophosphate," *Russ. J. Inorg. Chem.*, **21**, 1126–9 (1976).
[52]M. Stech, P. Reynders, and J. Rodel, "Constrained Film Sintering of Nanocrystalline TiO_2," *J. Am. Ceram. Soc.*, **83**, 1889–96 (2000).
[53]M. N. Rahaman, *Ceramic Processing and Sintering*. Marcel Dekker Inc., New York, 1995.
[54]N. Maazi and N. Rouag, "Consideration of Zener Drag Effect by Introducing a Limiting Radius for Neighbourhood in Grain Growth Simulation," *J. Crystal Growth*, **243**, 361–9 (2002).
[55]E. Nes, N. Ryum, and O. Hunderi, "On the Zener Drag," *Acta Metall.*, **33**, 11–22 (1985).
[56]M. N. Rahaman, R. E. Dutton, and S. L. Semiatin, "Effect of Solid Solution Additives on the Densification and Creep of Granular Ceramics," *Acta Mater.*, **45**, 3017–28 (1997).
[57]N. Moelans, B. Blanpain, and P. Wollans, "Pinning Effect of Second-Phase Particles on Grain Growth in Polycrystalline Films Studied by 3-D Phase Field Simulations," *Acta Mater.*, **55**, 2173–82 (2007).
[58]E. E. Boakye, R. S. Hay, M. D. Petry, and T. A. Parthasarathy, "Zirconia–Silica–Carbon Coatings on Ceramic Fibers," *J Am. Ceram. Soc.*, **87**, 1967–76 (2004).
[59]R. S. Hay, E. E. Boakye, and M. D. Petry, "Effect of Coating Deposition Temperature on Monazite Coated Fiber," *J. Eur. Ceram. Soc.*, **20**, 589–97 (2000). □